





Anticancer Agents

International Edition: DOI: 10.1002/anie.201913087 German Edition: DOI: 10.1002/ange.201913087

Supramolecular Design of Unsymmetric Reverse Bolaamphiphiles for Cell-Sensitive Hydrogel Degradation and Drug Release

Rami W. Chakroun, Alexandra Sneider, Caleb F. Anderson, Feihu Wang, Pei-Hsun Wu, Denis Wirtz, and Honggang Cui*

Abstract: Self-assembly of peptide-based building units into supramolecular nanostructures creates an important class of biomaterials with robust mechanical properties and improved resistance to premature degradation. Yet, upon aggregation, substrate-enzyme interactions are often compromised because of the limited access of macromolecular proteins to the peptide substrate, leading to either a reduction or loss of responsiveness to biomolecular cues. Reported here is the supramolecular design of unsymmetric reverse bolaamphiphiles (RBA) capable of exposing a matrix metalloproteinase (MMP) substrate on the surface of their filamentous assemblies. Upon addition of MMP-2, these filaments rapidly break into fragments prior to reassembling into spherical micelles. Using 3D cell culture, it is shown that drug release is commensurate with cell density, revealing more effective cell killing when more cancer cells are present. This design platform could serve as a cell-responsive therapeutic depot for local chemotherapy.

Introduction

Low-molecular-weight surfactants^[1] and macromolecular surfactants^[2] such as block copolymers are known to form a great diversity of discrete supramolecular morphologies in solution, and nanostructured materials in bulk.^[3] Conventionally, amphiphiles are linear molecules formed by covalent linkage of a hydrophobic moiety to a either hydrophilic headgroup or segment. To create more sophisticated functionalities, the molecular design of linear amphiphiles has evolved over the past three decades to those containing various functional units and those with complex chain architectures.^[4] For example, branched amphiphiles such as mikto-arm star block copolymers^[5] or dendritic amphiphiles^[6]

have been developed, consisting of multiple hydrophobic and hydrophilic segments. Linear bolaamphiphiles with symmetric^[7] and asymmetric^[8] designs have also been investigated, forming a variety of morphologies. Dendritic bolaamphiphiles are another important class of branched molecules possessing a central hydrophobic region with hydrophilic dendrons at each terminal.^[9] These innovative amphiphile designs have expanded the morphology library and functional space of classical surfactant assembly, leading to the discovery of a plethora of interesting nanostructures with unique functionalities. [9a,b,10] In addition to architecture variations, numerous functional units have also been introduced to the amphiphile design.^[11] One notable example is the peptide amphiphiles (PAs) that exploit both the structural and biological roles of small-molecule peptides to construct protein analogous micelles^[11c,d,12] and biologically active peptide amphiphile nanofibers.^[13] Along the lines, the incorporation of therapeutic agents creates an emerging class of self-assembling prodrugs, termed drug amphiphiles (DA), that can assume a variety of supramolecular morphologies in aqueous environment.^[14] It is in this context that we report a reverse bolaamphiphile (RBA) design with asymmetric hydrophobic units as terminal groups to enable specific enzyme- and cellresponsive hydrogel degradation and drug release.

Abnormal enzymatic activities are implicated in many human diseases such as cancer and represent a popular target for disease treatment.^[15] In particular, the expression and release of matrix metalloproteinases (MMPs) is linked to tumor aggressiveness and metastasis, [15a, 16] and has been a subject of heavy interest in the development of enzymeresponsive biomaterials. For instance, the group of Xu pioneered the use of enzymes as a trigger for self-assembly into biologically relevant nanomaterials. [17] For MMP-responsiveness, it has been demonstrated by a number of groups that the enzymatic cleavage at a monomeric level either transforms the molecule into an effective hydrogelator^[18] or triggers a change in nanostructure morphology.^[19] From the perspective of molecular design, success of this strategy relies heavily on the accessibility of the enzyme to the target molecular substrate, which occurs easily in its monomeric state but is greatly hindered in the assembled state. One way to overcome this issue is through post-assembly crosslinking, where the cleavage sites are chemically conjugated onto the peptide nanostructures, ensuring surface degradation.[20] However, this method suffers from the complicated procedure of crosslinking chemistry and subsequent removal of the potentially toxic initiators. Another method is to incorporate MMP degradable sequences into the main peptide design

Department of Chemical and Biomolecular Engineering, and Institute for NanoBiotechnology, The Johns Hopkins University 3400 North Charles Street, Baltimore, MD 21218 (USA) E-mail: hcui6@jhu.edu

P.-H. Wu, Prof. D. Wirtz, Prof. H. Cui

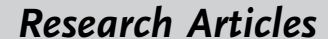
Department of Oncology and Sidney Kimmel Comprehensive Cancer Center, Johns Hopkins University School of Medicine 400 North Broadway, Baltimore, MD 21231 (USA)

Prof. H. Cui

Center for Nanomedicine, The Wilmer Eye Institute, Johns Hopkins University School of Medicine (USA)

Supporting information and the ORCID identification number(s) for the author(s) of this article can be found under: https://doi.org/10.1002/anie.201913087.

^[*] R. W. Chakroun, A. Sneider, C. F. Anderson, F. Wang, P.-H. Wu, Prof. D. Wirtz, Prof. H. Cui







such as RADA peptides, [21] multi-domain peptides, [22] and β -hairpin peptides [23] to form enzyme-responsive hydrogel systems. However, in these systems, it is not clear whether disassembly is a result of MMPs acting on the fibers themselves, or a compensation for the shift in the equilibrium balance between monomers and their respective assemblies. Herin, we demonstrate the importance of RBA design in exposing the MMP-2 cleavable sequence on the filament surface. Through a series of two- and three-dimensional (2D and 3D) in vitro experiments, we illustrate the functionality and efficiency of the self-assembling RBA hydrogel system as a supramolecular local depot for their specific response to enzymes and enzyme-expressing cancer cells.

Results and Discussion

Molecular Design and Assembly

The reverse peptide bolaamphiphile reported here consists of a hydrophilic peptide and an MMP cleavable peptide in the middle with two hydrophobic terminals that are structurally different: the C-terminus contains a triple valine sequence, while the N-terminus is a twelve-carbon alkyl chain (Figure 1). Valine was chosen because of its known high propensity to form β -sheet conformations, $^{[24]}$ and also because

our previous studies suggested that valine represents a strong contributor to filament formation. [25] The first part of the hydrophilic segment consists of Arg-Gly-Asp-Arg, which helps promote solubility through multiple charged amino acids. The second part serves as the MMP cleavable sequence, Pro-Leu-Gly-Val-Arg (PLGVR). [26] This substrate has a $K_{\rm m}$ value of 290 μ m and $K_{\rm cat}$ value of 4.1 s⁻¹ for MMP-2, with the cleavage site between G and V. [26] Upon MMP-2 cleavage, it is expected that removal of the peptide, Val-Arg-Val-Val-Val sequence, from the RBA-1 would significantly weaken the intermolecular interactions so as to alter the assembly landscape. Details of synthesis, purification, and characterization of all the studied molecules can be found in the Supporting Information (see Figures S1–S9).

In our experiments to study its assembly and MMP responsiveness, RBA-1 was first dissolved in water at a concentration of 2 mm, and the solution was then heated to 80 °C for one hour and left overnight. Transmission electron microscopy (TEM) imaging reveals dominant filamentous structures (Figure 2 A). Upon the addition of PBS, the RBA-1 solution was triggered to form a self-supporting hydrogel (Figure 2B). In the presence of 0.2 μ g of MMP-2 enzyme (0.01 mg mL⁻¹ in PBS), the hydrogel was observed to break down completely within 24 hours (Figure 2B). We also synthesized the molecule that would be formed after MMP cleavage of the PLG*VR (C_{12} -GGRGDRPLG) where *

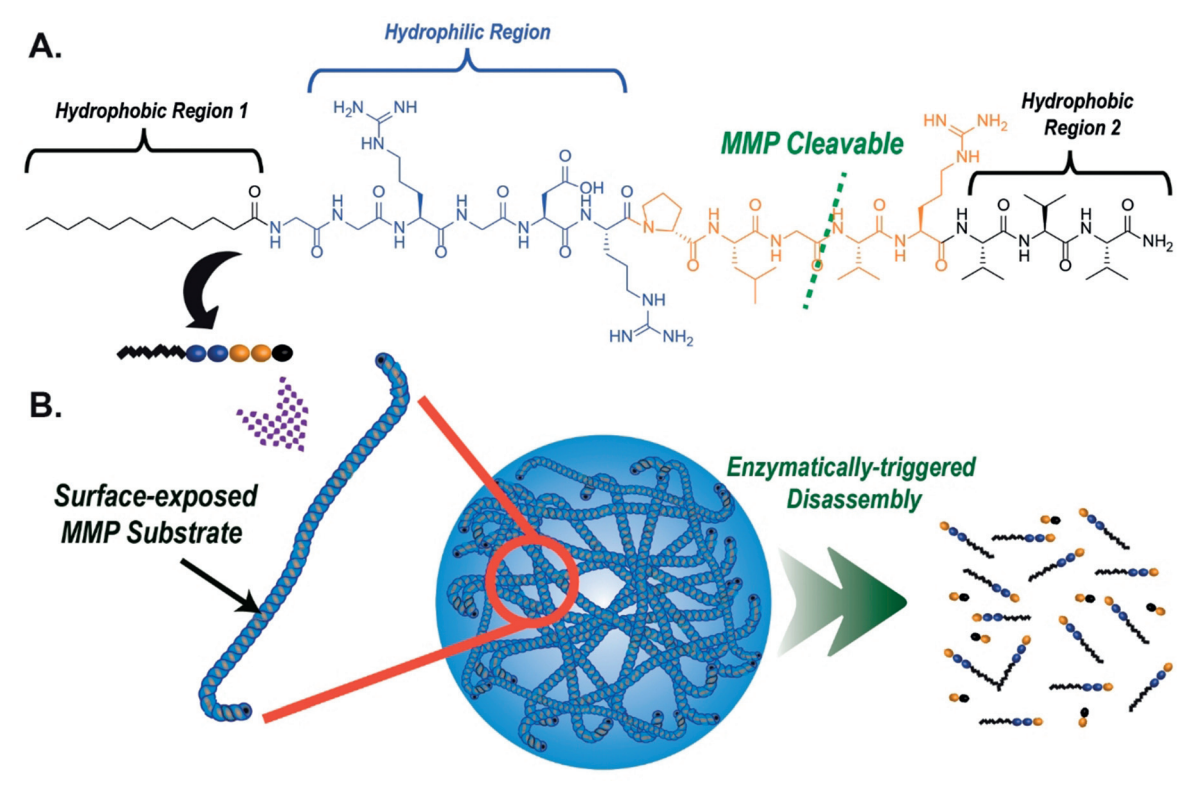


Figure 1. Molecular design and assembly of unsymmetric reverse bolaamphiphile (RBA-1). A) Chemical structure of a representative RBA-1 design with two different hydrophobic ends (black) consisting of an alkyl chain on the N-terminus (region 1), a triple valine sequence on the C-terminus (region 2) and, a hydrophilic region (blue) consisting of a double glycine spacer and an RGDR sequence, and an MMP-2 cleavable sequence PLGVR (orange). B) The RBA-1 monomers assemble into supramolecular filaments in water with the MMP-2 substrates displayed on the surface. At either elevated concentrations or in the presence of counterions, these filaments entangle into a hydrogel. Upon exposure to enzymes or enzyme-expressing cells, the supramolecular filament hydrogel is expected to break down, with the possibility of reassembly by the cleaved molecule.



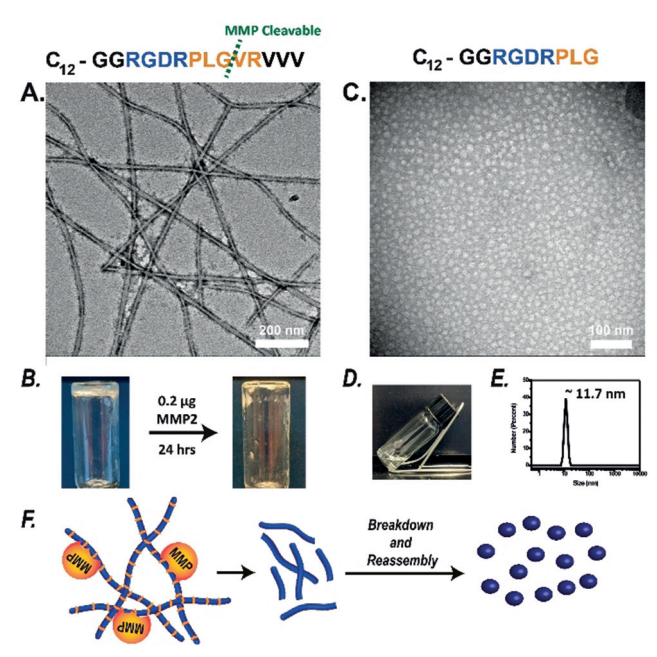


Figure 2. Self-assembly and degradation characteristics of our RBA-1 molecule. A) TEM micrograph of the supramolecular filaments formed. B) Gel images before and after MMP-2 treatment of 0.2 μg enzyme (0.01 mg mL $^{-1}$ in PBS), aged at 37°C. Upon addition of charge-screening phosphate buffer saline (PBS) directly after aging in water, the molecule spontaneously formed a hydrogel. C) Cleaved RBA-1 control molecule resembling the segment that would be left after cleavage of our original design displayed spherical micelle morphology using TEM. D) No hydrogel formation was observed after addition of PBS. E) DLS measured 11.7 nm particles. The molecules were dissolved in water and heated at 80°C for 1 hour, after which they were aged for 1 day at a 2 mm concentration before carrying out either TEM, DLS, or gel formation and degradation studies. F) Descriptive illustrations for our main reverse bolaamphiphile design breaking down and reassembling into spherical micelles.

denotes the target cleavage site. This cleaved RBA-1 control molecule exhibited no gelation capabilities when subjected to

PBS, forming spherical micelles of about 11.7 nm diameter upon aging in water at а 2 mм concentration (Figures 2C-E). Circular dichroism (CD) spectra of this cleaved RBA-1 control revealed a random coil secondary structure, as evident by the negative peak at about 200 nm (see Figure S10). These results demonstrate the importance of including a valine-rich peptide in the C-terminus of RBA-1 design to facilitate the filamentous growth. The formation of spherical assemblies after enzymatic removal may account for the hydrogel breakdown illustrated in Figure 2F.

Enzyme Degradation

To develop a deeper understanding of the hydrogel breakdown process, TEM and CD studies were carried out on RBA-1 hydrogels at different time points after the addition of MMP-2. Initially, RBA-1 showed great gelation capabilities (Figure 3A) with dominant filamentous nanostructures observed throughout the TEM grid (Figure 3B). The CD spectrum of the molecule (see Figure S11) displayed a negative peak around 220 nm, attributed to intermolecular hydrogen bonding among peptides. After 24 hours of MMP-2 treatment, the hydrogel became a cloudy suspension of gel particles. TEM displayed longer filaments accompanied by numerous shorter fragments (see Figure S12). Concurrently, the CD data displayed a decrease in the β -sheet peak and a sign of random coil absorption, as indicated by a minor negative peak shown at about 205 nm. Upon further aging for additional 48 hours, spherical assemblies were observed, similar to those formed by the control molecule (Figure 2B). As expected, the CD study revealed random coils as the dominant secondary structure. After a total of 72 hours of MMP treatment, a sample solution of the final product was removed and measured using MALDI (see Figure S16), and the peak corresponding to the RBA-1 molecular mass was found to be replaced with multiple other peaks, including the expected cleaved molecule (G*V). The production of other species is likely a result of the cleaved molecule undergoing further degradation by the MMP enzyme.

The RBA-1 gelation behavior and rheological properties before and after MMP-2 treatment were also assessed using an oscillatory time-sweep test (see Figure S13). Before PBS addition, the RBA-1 filaments demonstrated solution-like rheological properties while the addition of $10 \times PBS$ at the 150 s time point resulted in an increase in the storage modulus (G') and stabilization of the loss modulus (G''), with the crossover point (G' > G'') occurring at about 170 seconds (i.e. 20 s after PBS treatment), suggestive of forming a gel. The stiffness of the gel was observed to increase slightly with time.

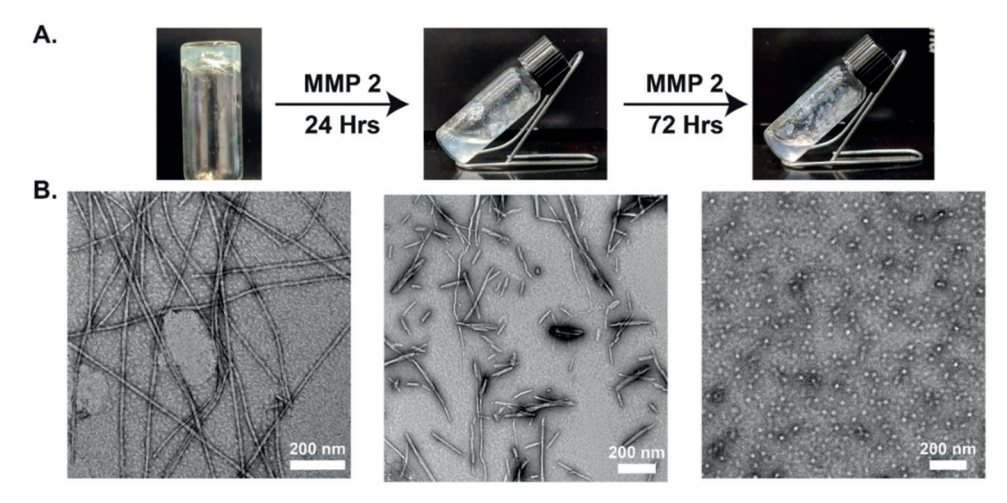


Figure 3. MMP-2 triggered RBA-1 supramolecular filament breakdown and re-assembly of the fragmented RBA-1 at different time points. A) Gel images of the RBA-1 molecule at different time points (0 h, 24 h and 72 h) after being treated with 0.2 μg (0.01 mg mL $^{-1}$ in PBS) of MMP-2 enzyme. B) The respective TEM images display the breakdown of the originally formed filaments into smaller ones, followed by re-assembly of the fragmented RBA-1 into spherical micelles.



After 24 hours of treatment with a large amount of MMP-2, the rheology test clearly suggested a transition back to solution phase, as evidenced by a destabilization of the storage modulus (G') and loss modulus (G'').

The key in developing enzyme-responsive supramolecular filaments is the presentation of the cleavage site to the target enzyme. Using a traditional amphiphilic design, the cleavage site would either largely remain embedded within the core or become overly crowded in the corona, not easily accessible to macromolecular proteins. The formation of shortened filaments in Figure 3 after 24 hours of treatment with the MMP-2 enzyme, provides indirect evidence for concurrent cleavage on the filament surface, not only on the monomeric units that shift the assembly equilibrium. If the latter case dominated the cleavage mechanism, one would expect to observe a large population of spherical assemblies, instead of shortened filaments, formed by the cleaved molecule.

To further understand the cleavage mechanism and specificity, we synthesized two more control molecules shown in Figure 4. In the first molecular design, the triple valine sequence originally on the C-terminus of the peptide was shifted towards the N-terminus while the hydrophilic RGDR was moved to the C-terminus. The resultant molecule can assemble into filamentous structures, as shown by TEM imaging (Figure 4A). However, even after aging with MMP-2 for two weeks, no noticeable sign of hydrogel degradation was

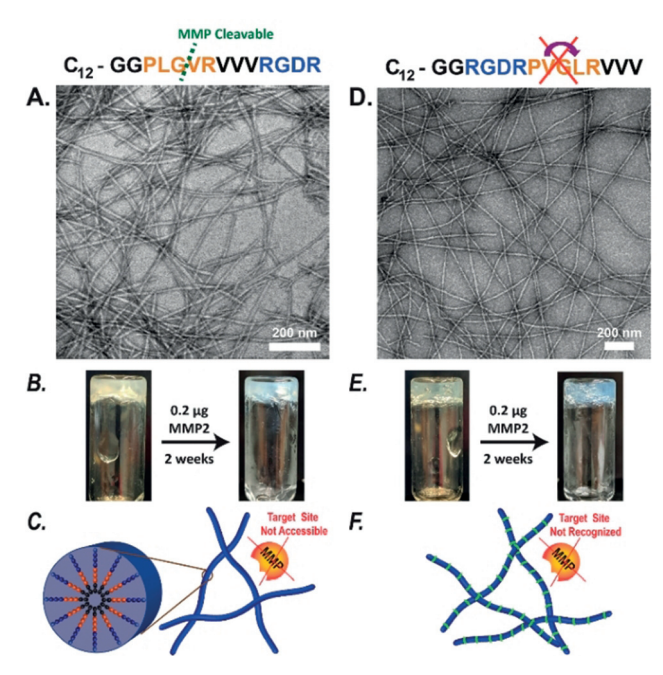


Figure 4. Resistance to enzyme degradation of two control molecules to highlight the significance of RBA-1 design. A) Traditional linear amphiphile design by placing the RGDR hydrophilic peptide at the Cterminus (PA-1 control), and B) RBA-1 design with a modified noncleavable MMP substrate (Scrambled RBA-1 control). A,D) TEM images of the filaments formed assembly of the respective molecules. B,E) Gel images before and after MMP-2 treatment of 0.2 µg enzyme, aged at 37 °C. and C,F) Descriptive illustrations. Gelation was triggered by the addition of phosphate buffer saline (PBS). Both molecules were treated the same as our original design: dissolved at 2 mM concentration in water and heated at 80 °C for 1 hour, then aged for 1 day.

observed by naked eyes (Figure 4B). This result further confirms the significance of the reverse bolaamphiphile design that enables the display of the MMP-2 substrate on the filament surface. It is reasonable to assume that after selfassembly, the MMP-2 substrate incorporated in the PA-1 would be embedded within the resultant filaments, inaccessible to macroscale enzymes. Given that both molecules exhibit low critical micelle concentrations (see Figure S14), only a very small percentage of monomer exists in solution and thus cleavage by MMP on the monomeric units is not expected to contribute significantly to the hydrogel degradation process. To provide more insight into the MMP cleavage process, Nile Red was used to compare filament cleavage difference in the RBA-1 and PA-1 assemblies (see Figure S15). When encapsulated in a hydrophobic environment, Nile Red emits at 635 nm as opposed to 660 nm in aqueous solution. Since spherical micelles accommodate more Nile Red (see Figure S15B), the rate of filament breakdown by MMP-2 would be reflected by an increase in fluorescence signal at 635 nm as a result of forming spherical micelles that accommodate more Nile Red. As shown in Figure S15C, adding MMP into RBA-1 filaments led to a rapid increase, over time, in Nile Red encapsulated within the micelles, reaching a plateau after 24 hours. In comparison, PA-1 did not reveal any significant change in encapsulation over the period of 72 hours.

In the second molecular design, we replaced the PLGVR with a scrambled PVGLR sequence (presumably not cleavable by MMP). This molecule also forms a supramolecular filament hydrogel, and again, no disassembly or hydrogel breakdown was observed upon aging with MMP-2 enzyme (Figure 4A,B). MALDI further confirmed the resistance of both PA-1 and Scrambled RBA-1 hydrogels for MMP responsiveness and chemical breakdown (see Figure S16). Collectively, these experiments suggest that the PLGVR sequence of the RBA-1 in the assembled states can be accessed and effectively cleaved by target MMP.

Hydrogel Degradation by Enzyme-Expressing Cells

We next investigated the degradability of the RBA-1 supramolecular hydrogel by MMP-expressing cells. It has been previously shown that certain cancer cell types at higher densities in 3D collagen type I matrices tend to secrete more MMPs than those at lower densities.^[12a] We therefore cultured the highly metastatic breast cancer MDA-MB-231 cell line in a 3D in vitro collagen environment at a high cell density (100000 cells mL⁻¹). Over a 72 hour period, cells were allowed to migrate, communicate, express MMPs, and proliferate. After 72 hours, the cell media of each plate were removed and added to the top of our MMP-2 responsive hydrogel. Fresh cell medium was used as a control. After two weeks, the hydrogel treated with the media showed significant breakdown. After four weeks, numerous fragmented hydrogel pieces can be observed to suspend in the solution, indicative of a bulk erosion mechanism enabled by cellexpressed MMPs. For degradation mechanism dominated by monomer cleavage, we would expect the cleavage reaction to







be heavily dependent upon the monomer dissociation kinetics from supramolecular filaments. This dissociation-dependent release often led to an apparent surface erosion mechanism. ^[25] In comparison, the control media showed no noticeable changes, even up to four weeks, and neither PA-1 nor Scrambled RBA-1 hydrogels showed visual signs of degradation (see Figure S17). Since the enzymatic reaction is concentration-dependent and MMPs are typically expressed by cells at much lower concentrations, ^[27,28] slower degradation rates were expected and observed in these experiments relative to the results reported in Figures 2, 3, and 4. The change in color observed after four weeks could be a result of proteins denaturing and/or degradation within the cell media.

To further demonstrate the specificity of our hydrogel to MMPs, we carried out experiments using an MMP inhibitor, Batismastat, to block the MMP activities (see Figure S17). Our results suggest that upon inhibition of MMP function no RBA-1 hydrogel degradation was observed. On basis of these obervations, we can confirm that degradation of the RBA-1 hydrogel in Figure 5 is a result of MMP cleavage as opposed to other nonspecific proteolysis reactions. Given that MMPs expressed by cancer cells can accelerate the breakdown of our hydrogel, we speculate this cell-responsive characteristic can be usesful in an in vivo setting to treat tumors of various sizes and aggressiveness.

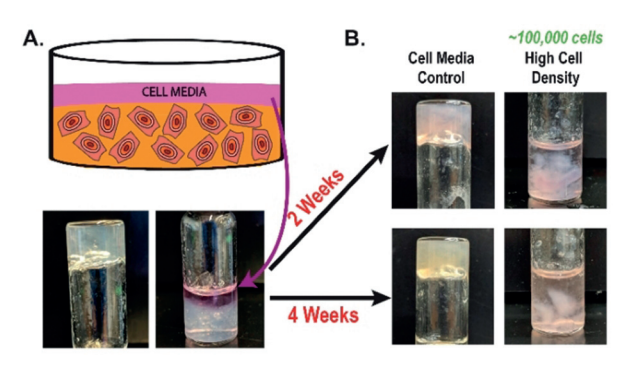


Figure 5. Surface erosion of our RBA-1 hydrogel treated with cell-expressed MMP. A) Metastatic breast cancer cell lines, MDA-MB-231, were cultured by imbedding them within a collagen gel matrix, to mimic a 3D environment. The cell media used to replenish the cells was removed from the top of the collagen matrix with high cell density (100,000 cells) and placed on the top of our reverse bolaamphiphile gel (B). At 2 and 4 week time points, gel images were taken to demonstrate the difference in degradation speed of our hydrogel under high cell density cell environments and a control consisting of fresh cell media.

Drug-Based RBA Design and Assembly

Inspired by the cell-regulated hydrogel breakdown, we sought to validate the use of the RBA design in controlled drug release. In this context, paclitaxel was chosen and conjugated to the N-terminus of our RBA peptide to replace the alkyl tail. A reducible disulphide linker (buSS) was used to bridge the drug to the peptide and also to facilitate the release of free drug after cell internalization. Figure 6A displays the chemical structure of the drug-based reverse

bolaamphiphile (DRBA-1). The hydrophilic Arg-Gly-Asp-Arg was substituted with a more charged Arg-Asp-Arg-Asp sequence to help counter solubility issues. In an in vitro assay, MDA-MB-231 cells were, respectively treated with the monomeric form of our DRBA-1 and free PTX at different concentrations (Figure 6B; see Figure S18). We observed comparable cytotoxicity between both drug molecules; DRBA-1 and free PTX exhibited an IC₅₀ value of 56 nm and 29 nm, respectively. These results imply the efficient reduction of the buSS linker by cells, maintaining the cytotoxic potency of the DRBA-1. In addition, RBA-1 and its major cleaved product, RBA-1 control, did not exhibit any noticeable effect on cell viability under the studied conditions (see Table S1). Our in vitro studies also suggest the potential use of RBA-1 hydrogels as coatings for 2D cell culture (see Figure S19).

To confirm its cell-responsive breakdown, the DRBA-1 hydrogel was treated with 0.2 μg of MMP-2 (0.01 mg mL⁻¹ in PBS) and analyzed at different time points using TEM (Figure 6D) and CD (see Figure S7B). In these experiments, the DRBA-1 monomers were dissolved in water at a 2 mm concentration. After aging overnight, TEM imaging displayed long and flexible filamentous structures capable of forming a hydrogel upon addition of PBS. These filaments displayed a strong dominant β -sheet peak at about 220 nm in the CD spectrum along with a strong positive peak at about 237 nm, corresponding to the paclitaxel absorbtion. Similar to the previous studies on RBA-1, these filaments were also observed to break down into shorter fragments after 24 hours in an enzyme environment, eventually converting into a solution form (Figure 6D). CD spectra displayed mixed absorption of random coils and β -sheet, indicating the cleavage of the triple-valine segment and a change in assembly hehavior. After a total of 72 hours of incubation, only spherical micelles could be observed according to TEM imaging, and the random coil secondary structure measured dominated the collected CD spectra. MALDI-TOF studies (see Figure S16) revealed the dissapearance of the original DRBA-1 molecular mass, again confirming the action of the enzyme. The consistency of these results with the previous RBA-1 studies further confirms the ability of our sytem to retain its self-arranged structure and enzyme sensitivity, independent of the hydrophobic segment used.

Cell-Controlled Drug Release

To further demonstrate the enhanced cytotoxicity in response to cell density, we developed an in vitro 3D cell assay (Figure 7). The hydrogels used in these experiments were created by mixing DRBA-1 with RBA-1 at a molecular ratio of 1 to 4. A drop of 20 µL mixed solution was placed on a metal spatula, followed by gelation using PBS (Figure 7 A). Next, these hydrogel pellets were embedded within a collagen matrix containing different densities of the breast cancer cells (MDA-MB-231). At specific time points (0, 24, 48 and 72 h), cells from different locations of the petri dish were removed and treated with Hoechst stain and propidium iodide to examine their viability. This assay enables us to measure drug distribution, represented by cell death, as a function of





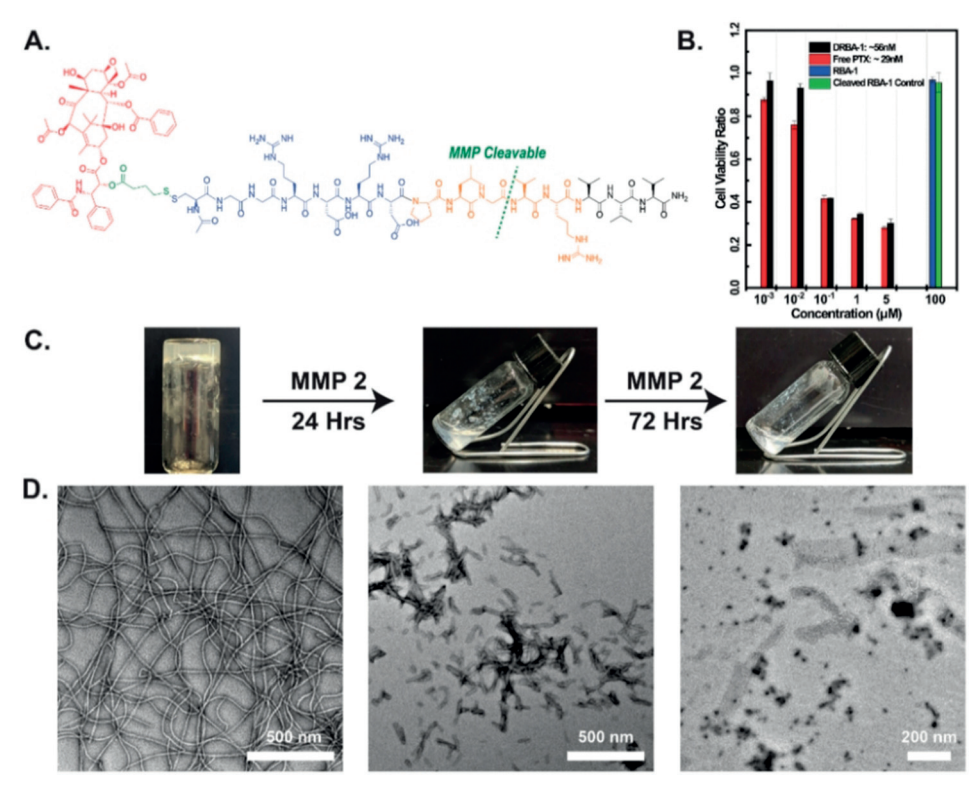


Figure 6. The design, assembly, and enzyme responsiveness of a drug-bearing RBA (DRBA-1). A) Chemical structure of the drug version of our reverse bolaamphiphile design with the alkyl chain of our peptide amphiphile (PA) replaced with paclitaxel (red), and RDRD serving as the hydrophilic region (blue). All other design features remain similar to that of RBA-1. B) Cytotoxicity comparison of our DRBA-1 with free PTX at different concentration, in MDA-MB-231 breast cancer cells. RBA-1 and cleaved RBA-1 control was also tested. Cells were incubated with the PTX or conjugates for 72 h and cell viability was determined by MTT assay. Values of 56 nM and 29 nM represent the IC50 value. Data are given as mean \pm s.d. (n=3). C) Gel images of our drug amphiphile at different time points (0 h, 24 h and 72 h) after being treated with 0.2 μg of MMP-2 enzyme (0.01 mg mL $^{-1}$ in PBS). The respective TEM images (D) for each time point display the breakdown of the original filaments into smaller fragments, followed by reassembly into spherical micelles. To form the filaments, the DRBA-1 was dissolved at 2 mM and heated for 1 h at 80°C followed by overnight aging. After the addition of PBS, the filament solution solidified into a gel, from which the TEM, CD and degradation studies were conducted.

position and time. As seen in Figures 7B-D, in a lower cell (10000 cells mL⁻¹) density environment, cell death was localized to areas around the hydrogel, whereas in a higher cell (100 000 cells mL⁻¹) density, an expanding impact to cells farther away was observed as time progressed. At a higher cell density, cells at the far end of the well exhibited an increase in cell death over time, showing 78 % viability over 72 hours. In a low cell density environment no cell death was observed beyond areas prominent to the gel even after 72 hours of treatment. We attribute the difference in cell killing to the MMP-responsive nature of our hydrogel and its ability to degrade more rapidly in the presence of an elevated level of MMP. In an environment with a larger number of cancer cells, more MMP will result in a faster breakdown of the RBA/ DRBA hydrogel, leading to more rapid drug release. This elevated drug level may also promote a deeper distribution into the tumor intersitium, attributed to the spherical morphology of the cleaved DRBA-1 product after cleavage. In an environment with fewer cancer cells, the RBA hydrogel will not breakdown as fast because of the limited MMP supplies, and the drug release will be restricted to adjacent areas around the hydrogel.

A proposed action of mechanism of DRBA-1 is illustrated in Figure 7F, showing the multipe stages of cell-controlled release of the therapeutic agents. Upon MMP cleavage, DRBA-1 filaments could fragment into short pieces that eventaully dissociate into monomeric drug amphiphiles. Delivering paclitaxel in the form of shortened filaments and/or potentially the reassembled spherical assemblies, as opposed to the monomeric individual drug conjugates, could lead to an enhanced distribution throughout the tumor intersitium with a better controlled drug release, as revealed by other groups.[29] Furthermore, drugs in the nanoparticle form could exhibit an enhanced cellular uptake and are also protected from rapid breakdown.[30] intracellular Nanoparticles could also help overcome multi-drug resistance.[31] Although we have yet to demonstrate all these features in our current studies, it is reasonable to assume that the potentially reassembled nanoparticles may exhibit some of these properties. This potential is evident in our 3D in vitro

studies, which not only show a tumor-responsive drug release, but for a limited amount of drug, a higher percentage of cell death was observed in areas with a greater cell density.

Conclusion

In summary, we have designed and synthesized peptide-based reverse bolaamphiphiles with unsymmetric hydrophobic segments, and demonstrated the importance of the reverse bolaamphiphile design in constructing enzyme-responsive supramolecular filament hydrogels with effective display of MMP-2 substrate on the surface. By replacing the hydrocarbon with an anticancer drug, we developed a drug-based RBA hydrogel with potentially improved cancer treatment capabilities. Our in vitro 3D cell studies revealed a greater drug release rate and more effective cancer cell killing when a higher density of cancer cells were present as a result of an increased level of MMP expression. We believe this RBA design plaform is a new addition to the amphiphile family, and

4439

Research Articles





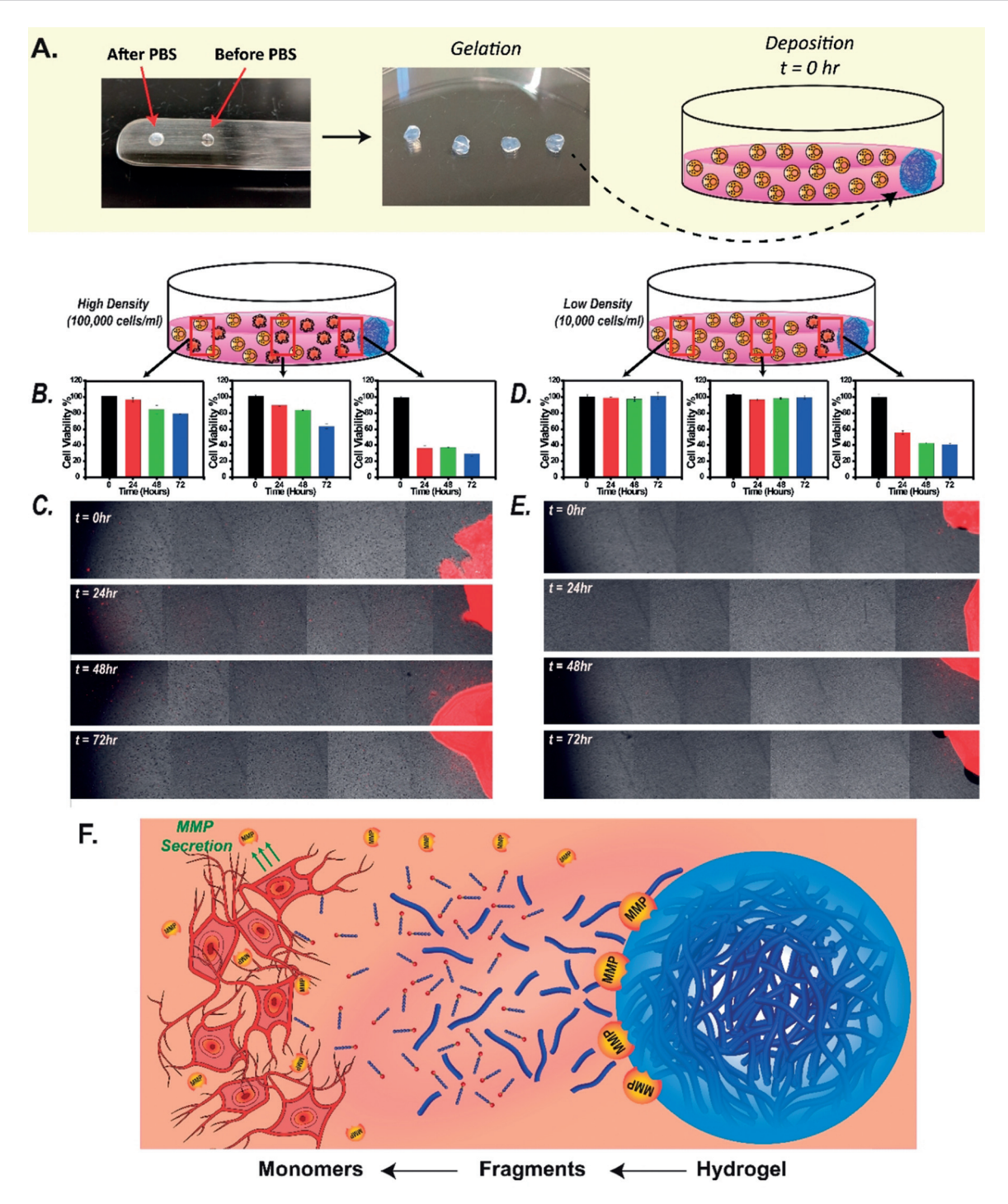


Figure 7. Controlled release of paclitaxel by enzyme-expressing cancer cells. A) Illustration detailing the setup procedure for our 3D in vitro cell studies. 20 μL droplets of 20% drug loading were placed on a metal spatula and PBS was added to trigger gelation, producing solid gel pieces of similar gel volume. The gel pieces were then deposited within a 3D collagen matrix of different cell densities. The release kinetics and cytotoxic effect of our hydrogel under high and low cell densities was assessed. Our gel was implanted in the collagen matrix containing an equal distribution of MDAMB 231 cells at different densities. The hydrogel was placed on one side of the well and both quantitative (B, D) and qualitative (C, E) data was obtained revealing cell death across the matrix, away from the gel, at different time points. Separate plates were prepared for analysis of each time point, at which cells were stained with Hoechst and propidium iodide, and then imaged. Data are given as mean \pm s.d (n=3). F) Schematic Illustration depicting the fragmentation of filaments within our hydrogel upon contact with MMP-2 enzyme, into monomers followed by their consequent diffusion throughout the tumor microenvironment.

envision that after further optimization a selective release of chemotherapeutic agent can be achieved in response to the tumor size and aggresiveness, thus enabling improved local treatment of cancer.

Research Articles





Acknowledgements

The work reported here is supported by the National Science Foundation (DMR 1255281) and 1746891 (Wirtz). R.W.C. and A.S. acknowledge the support from the NSF Graduate Research Fellowships Program (DGE 1746891). We also extend our sincere gratitude to the Integrated Imaging Center (IIC) for TEM imaging, the Mass Spectrometry Facility (MSF) for help acquiring high-resolution mass spectrometry data, and the Biomolecular NMR Center for acquisition of NMR spectra and consultation at Johns Hopkins University. In addition, we are thankful to Dr Siva P. Kambhampati and Dr Rangaramanujam M. Kannan for their help in obtaining and analyzing the rhelogical properties of our hydrogel.

Conflict of interest

The authors declare no conflict of interest.

Keywords: anticancer · drug delivery · hydrogels · nanostructures · self-assembly

How to cite: Angew. Chem. Int. Ed. **2020**, 59, 4434–4442 Angew. Chem. **2020**, 132, 4464–4472

- a) R. Zana, Y. Talmon, *Nature* 1993, 362, 228; b) C. Ni, P. A. Hassan, E. W. Kaler, *Langmuir* 2005, 21, 3334–3337.
- [2] a) L. Zhang, A. Eisenberg, Science 1995, 268, 1728-1731; b) Y. He, Z. Li, P. Simone, T. P. Lodge, J. Am. Chem. Soc. 2006, 128, 2745-2750; c) H. Che, J. Zhu, S. Song, A. Mason, S. Cao, I. Pijpers, L. Abdelmohsen, J. van Hest, Angew. Chem. Int. Ed. 2019, 58, 13113-13118; Angew. Chem. 2019, 131, 13247-13252.
- [3] S. Kim, P. F. Nealey, F. S. Bates, ACS Macro Lett. 2012, 1, 11–14.
- [4] M. Black, A. Trent, Y. Kostenko, J. S. Lee, C. Olive, M. Tirrell, Adv. Mater. 2012, 24, 3845 – 3849.
- [5] Z. Li, E. Kesselman, Y. Talmon, M. A. Hillmyer, T. P. Lodge, Science 2004, 306, 98–101.
- [6] V. Percec, A. E. Dulcey, V. S. Balagurusamy, Y. Miura, J. Smidrkal, M. Peterca, S. Nummelin, U. Edlund, S. D. Hudson, P. A. Heiney, *Nature* 2004, 430, 764.
- [7] a) T. Shimizu, R. Iwaura, M. Masuda, T. Hanada, K. Yase, J. Am. Chem. Soc. 2001, 123, 5947-5955; b) M. Kogiso, Y. Okada, T. Hanada, K. Yase, T. Shimizu, Biochim. Biophys. Acta Gen. Subj. 2000, 1475, 346-352.
- [8] a) J. Guilbot, T. Benvegnu, N. Legros, D. Plusquellec, J.-C. Dedieu, A. Gulik, *Langmuir* 2001, 17, 613-618; b) J. H. Fuhrhop, D. Spiroski, C. Boettcher, J. Am. Chem. Soc. 1993, 115, 1600-1601; c) J. H. Fuhrhop, D. Fritsch, Acc. Chem. Res. 1986, 19, 130-137; d) R. C. Claussen, B. M. Rabatic, S. I. Stupp, J. Am. Chem. Soc. 2003, 125, 12680-12681.
- [9] a) H. Zeng, M. E. Johnson, N. J. Oldenhuis, T. N. Tiambeng, Z. Guan, ACS Cent. Sci. 2015, 1, 303-312; b) A. C. Eldredge, M. E. Johnson, N. J. Oldenhuis, Z. Guan, Biomacromolecules 2016, 17, 3138-3144; c) A. C. Eldredge, M. E. Johnson, Y. Cao, L. Zhang, C. Zhao, Z. Liu, Q. Yang, Z. Guan, Biomaterials 2018, 178, 458-466.
- [10] V. Percec, D. A. Wilson, P. Leowanawat, C. J. Wilson, A. D. Hughes, M. S. Kaucher, D. A. Hammer, D. H. Levine, A. J. Kim, F. S. Bates, *Science* 2010, 328, 1009–1014.
- [11] a) S. R. Bull, M. O. Guler, R. E. Bras, T. J. Meade, S. I. Stupp, Nano Lett. 2005, 5, 1–4; b) J. Zhou, B. Xu, Bioconjugate Chem.

- **2015**, 26, 987–999; c) T. Pakalns, K. L. Haverstick, G. B. Fields, J. B. McCarthy, D. L. Mooradian, M. Tirrell, *Biomaterials* **1999**, 20, 2265–2279; d) P. Berndt, G. B. Fields, M. Tirrell, *J. Am. Chem. Soc.* **1995**, 117, 9515–9522.
- [12] a) Y.-C. Yu, P. Berndt, M. Tirrell, G. B. Fields, J. Am. Chem. Soc. 1996, 118, 12515–12520; b) B. F. Lin, K. A. Megley, N. Viswanathan, D. V. Krogstad, L. B. Drews, M. J. Kade, Y. Qian, M. V. Tirrell, J. Mater. Chem. 2012, 22, 19447–19454.
- [13] a) W. Ji, Z. Álvarez, A. N. Edelbrock, K. Sato, S. I. Stupp, ACS Appl. Mater. Interfaces 2018, 10, 41046-41055; b) M. J. Webber, J. Tongers, M.-A. Renault, J. G. Roncalli, D. W. Losordo, S. I. Stupp, Acta Biomater. 2010, 6, 3-11; c) J. D. Hartgerink, E. Beniash, S. I. Stupp, Science 2001, 294, 1684-1688; d) S. Soukasene, D. J. Toft, T. J. Moyer, H. Lu, H.-K. Lee, S. M. Standley, V. L. Cryns, S. I. Stupp, ACS Nano 2011, 5, 9113-9121; e) J. B. Matson, S. I. Stupp, Chem. Commun. 2011, 47, 7962-7964; f) M. J. Webber, J. B. Matson, V. K. Tamboli, S. I. Stupp, Biomaterials 2012, 33, 6823-6832.
- [14] a) R. Lin, A. G. Cheetham, P. Zhang, Y.-a. Lin, H. Cui, *Chem. Commun.* 2013, 49, 4968–4970; b) A. G. Cheetham, P. Zhang, Y.-a. Lin, L. L. Lock, H. Cui, *J. Am. Chem. Soc.* 2013, 135, 2907–2910; c) P. Zhang, A. G. Cheetham, L. L. Lock, H. Cui, *Bioconjugate Chem.* 2013, 24, 604–613.
- [15] a) C. A. La Porta, S. Zapperi, Seminars in cancer biology, Elsevier, Amsterdam, 2018; b) H. D. Foda, S. Zucker, Drug Discovery Today 2001, 6, 478–482.
- [16] C. F. Anderson, H. Cui, Ind. Eng. Chem. Res. 2017, 56, 5761 5777.
- [17] a) H. Wang, Z. Feng, B. Xu, Angew. Chem. Int. Ed. 2019, 58, 5567–5571; Angew. Chem. 2019, 131, 5623–5627; b) Y. Gao, Y. Kuang, Z.-F. Guo, Z. Guo, I. J. Krauss, B. Xu, J. Am. Chem. Soc. 2009, 131, 13576–13577; c) H. Wang, Z. Feng, Y. Wang, R. Zhou, Z. Yang, B. Xu, J. Am. Chem. Soc. 2016, 138, 16046–16055.
- [18] a) Z. Yang, M. Ma, B. Xu, Soft Matter 2009, 5, 2546 2548; b) A. Tanaka, Y. Fukuoka, Y. Morimoto, T. Honjo, D. Koda, M. Goto, T. Maruyama, J. Am. Chem. Soc. 2015, 137, 770 775.
- [19] a) D. Kalafatovic, M. Nobis, N. Javid, P. W. Frederix, K. I. Anderson, B. R. Saunders, R. V. Ulijn, *Biomater. Sci.* 2015, 3, 246–249; b) D. Kalafatovic, M. Nobis, J. Son, K. I. Anderson, R. V. Ulijn, *Biomaterials* 2016, 98, 192–202; c) J. Son, D. Kalafatovic, M. Kumar, B. Yoo, M. A. Cornejo, M. Contel, R. V. Ulijn, *ACS Nano* 2019, 13, 1555–1562.
- [20] a) Y. Zhang, N. Li, J. Delgado, Y. Gao, Y. Kuang, S. Fraden, I. R. Epstein, B. Xu, *Langmuir* 2012, 28, 3063 3066; b) Y.-A. Lin, Y.-C. Ou, A. G. Cheetham, H. Cui, *Biomacromolecules* 2014, 15, 1419–1427; c) Y. Zhang, R. Zhou, J. Shi, N. Zhou, I. R. Epstein, B. Xu, *J. Phys. Chem. B* 2013, 117, 6566–6573.
- [21] Y. Chau, Y. Luo, A. C. Cheung, Y. Nagai, S. Zhang, J. B. Kobler, S. M. Zeitels, R. Langer, *Biomaterials* 2008, 29, 1713–1719.
- [22] K. M. Galler, L. Aulisa, K. R. Regan, R. N. D'Souza, J. D. Hartgerink, J. Am. Chem. Soc. 2010, 132, 3217 – 3223.
- [23] M. C. Giano, D. J. Pochan, J. P. Schneider, *Biomaterials* 2011, 32, 6471–6477.
- [24] a) M. Levitt, Biochemistry 1978, 17, 4277 4285; b) P. Koehl, M. Levitt, Proc. Natl. Acad. Sci. USA 1999, 96, 12524 12529.
- [25] R. W. Chakroun, F. Wang, R. Lin, Y. Wang, H. Su, D. Pompa, H. Cui, ACS Nano 2019, 13, 7780 7790.
- [26] J. Seltzer, K. Akers, H. Weingarten, G. Grant, D. McCourt, A. Eisen, J. Biol. Chem. 1990, 265, 20409 – 20413.
- [27] a) Y. Liu, D. Zhang, Z. Y. Qiao, G. B. Qi, X. J. Liang, X. G. Chen, H. Wang, Adv. Mater. 2015, 27, 5034–5042; b) Z.-H. Peng, J. i. Kopeček, J. Am. Chem. Soc. 2015, 137, 6726–6729; c) C. Huang, Y. Sun, M. Shen, X. Zhang, P. Gao, Y. Duan, ACS Appl. Mater. Interfaces 2016, 8, 1360–1370.
- [28] L. Zhu, T. Wang, F. Perche, A. Taigind, V. P. Torchilin, *Proc. Natl. Acad. Sci. USA* 2013, 110, 17047–17052.

GDCh

Research Articles



- [29] a) G. Lambert, J. R. Bertrand, E. Fattal, F. Subra, H. Pinto-Alphandary, C. Malvy, C. Auclair, P. Couvreur, Biochem. Biophys. Res. Commun. 2000, 279, 401–406; b) G. Lambert, E. Fattal, H. Pinto-Alphandary, A. Gulik, P. Couvreur, Pharm. Res. 2000, 17, 707–714; c) P. Majumder, U. Baxa, S. T. Walsh, J. P. Schneider, Angew. Chem. Int. Ed. 2018, 57, 15040–15044; Angew. Chem. 2018, 130, 15260–15264.
- [30] a) I. Brigger, C. Dubernet, P. Couvreur, Adv. Drug Delivery Rev.
 2012, 64, 24-36; b) C. Chavany, T. Saison-Behmoaras, T. Le Doan, F. Puisieux, P. Couvreur, C. Hélène, Pharm. Res.
 1994, 11, 1370-1378; c) L. L. Lock, C. D. Reyes, P. Zhang, H. Cui, J. Am. Chem. Soc. 2016, 138, 3533-3540; d) X. Pepin, L. C.
- Attali, C. Domrault, S. Gallet, J. M. Metreau, Y. Reault, P. J. Cardot, M. Imalalen, C. Dubernet, E. Soma, *J. Chromatogr. B* **1997**, *702*, 181 191.
- [31] S. Bennis, C. Chapey, J. Robert, P. Couvreur, Eur. J. Cancer 1994, 30, 89–93.

Manuscript received: October 13, 2019 Revised manuscript received: December 2, 2019 Accepted manuscript online: January 13, 2020 Version of record online: January 30, 2020